Fine-tuned high-*Q* photonic-crystal nanocavity

Yoshihiro Akahane[1,2], Takashi Asano[1], Bong-Shik Song[1], and Susumu Noda[1]

[1] *Department of Electronic Science and Engineering, Kyoto University, Kyoto 615-8510, Japan*

[2] *Semiconductor Technologies R&D Laboratories, Sumitomo Electric Industries, Ltd., Itami, Hyogo 664-0016, Japan*

y-akahane@sei.co.jp, snoda@kuee.kyoto-u.ac.jp

Abstract: A photonic nanocavity with a high *Q* factor of 100,000 and a modal volume *V* of 0.71 cubic wavelengths, is demonstrated. According to the cavity design rule that we discovered recently, we further improve a point-defect cavity in a two-dimensional (2D) photonic crystal (PC) slab, where the arrangement of six air holes near the cavity edges is fine-tuned. We demonstrate that the measured *Q* factor for the designed cavity increases by a factor of 20 relative to that for a cavity without displaced air holes, while the calculated modal volume remains almost constant.

OCIS codes: (230.5750) Resonators; (230.3990) Microstructure devices

References and links

1. S. Noda, A. Chutinan, and M. Imada, "Trapping and emission of photons by a single defect in a photonic bandgap structure," Nature **407**, 608-610 (2000).
2. B. S. Song, S. Noda, and T. Asano, "Photonic devices based on in-plane hetero photonic crystals," Science **300**, 1537 (2003).
3. H. Takano, Y. Akahane, T. Asano, and S. Noda, "In-plane-type channel drop filter in a two-dimensional photonic crystal slab," Appl. Phys. Lett. **84**, 2226-2228 (2004).
4. M. Lončar, A. Scherer, and Y. Qiu, "Photonic crystal laser sources for chemical detection," Appl. Phys. Lett. **82**, 4648-4650 (2003).
5. O. Painter, R. K. Lee, A. Scherer, A. Yariv, J. D. O'Brien, P. D. Dapkus, and I. Kim, "Two-dimensional photonic band-gap defect mode laser," Science **284**, 1819-1821 (1999).
6. P. Michler, A. Kiraz, C. Becher, W. V. Schoenfeld, P. M. Petroff, L. Zhang, E. Hu, and A. Imamoğlu, "A quantum dot single-photon turnstile device," Science **290**, 2282-2285 (2000).
7. M. F. Yanik and S. Fan, "Stopping light all optically," Phys. Rev. Lett. **92**, 083901 (2004).
8. S. G. Johnson, S. Fan, A. Mekis, and J. D. Joannopoulos, "Multipole-cancellation mechanism for high-*Q* cavities in the absence of a complete photonic band gap," Appl. Phys. Lett. **78**, 3388-3390 (2001).
9. J. Vučković, M. Lončar, H. Mabuchi, and A. Scherer, "Design of photonic crystal microcavities for cavity QED," Phys. Rev. E **65**, 016608 (2001).
10. J. Vučković, M. Lončar, H. Mabuchi, and A. Scherer, "Optimization of the *Q* factor in photonic crystal microcavities," IEEE J. Quantum Electron. **38**, 850-856 (2002).
11. K. Srinivasan and O. Painter, "Momentum space design of high-*Q* photonic crystal optical cavities," Opt. Express **10**, 670-684 (2002), http://www.opticsexpress.org/abstract.cfm?URI=OPEX-10-15-670.
12. H. Y. Ryu, M. Notomi, and Y. H. Lee, "High-quality-factor and small-mode-volume hexapole modes in photonic-crystal-slab nanocavities," Appl. Phys. Lett. **83**, 4294-4296 (2003).
13. Y. Akahane, T. Asano, B. S. Song, and S. Noda, "High-*Q* photonic nanocavity in a two-dimensional photonic crystal," Nature **425**, 944-947 (2003).
14. K. Srinivasan, P. E. Barclay, M. Borselli, and O. Painter, "Optical-fiber-based measurement of an ultrasmall volume high-*Q* photonic crystal microcavity," Phys. Rev. B **70**, 081306 (2004).
15. A. Chutinan, M. Mochizuki, M. Imada, and S. Noda, "Surface-emitting channel drop filters using single defects in two-dimensional photonic crystal slabs," Appl. Phys. Lett. **79**, 2690-2692 (2001).
16. C. Manalatou, M. J. Khan, S. Fan, P. R. Villeneuve, H. A. Haus, and J. D. Joannopoulos, "Coupling of modes analysis of resonant channel add-drop filters," IEEE J. Quantum Electron. **35**, 1322-1331 (1999).
17. Y. Tanaka, T. Asano, Y. Akahane, B. S. Song, and S. Noda, "Theoretical investigation of a two-dimensional photonic crystal slab with truncated cone air holes," Appl. Phys. Lett. **82**, 1661-1663 (2003).
18. B. Gayral, J. M. Gérard, A. Lemaître, C. Dupuis, L. Manin, and J. L. Pelouard, "High-*Q* wet-etched GaAs microdisks containing InAs quantum boxes," Appl. Phys. Lett. **75**, 1908-1910 (1999).

#6356 - $15.00 US Received 19 January 2005; revised 9 February 2005; accepted 11 February 2005

19. J. M. Gérard, B. Sermage, B. Gayral, B. Legrand, E. Costard, and V. Thierry-Mieg, "Enhanced spontaneous emission by quantum boxes in a monolithic optical microcavity," Phys. Rev. Lett. **81**, 1110-1113 (1998).
20. M. Fujita and T. Baba, "Microgear laser," Appl. Phys. Lett. **80**, 2051-2053 (2002).
21. B. S. Song, S. Noda, T. Asano, and Y. Akahane, "Ultrahigh-*Q* photonic double-heterostructure nanocavity," Nature Materials (to be published).

1. Introduction

Photonic cavities having dimensions of the order of optical wavelengths that can confine light strongly are very important for a variety of scientific and engineering applications, including ultra-small filters [1-3], high-resolution sensors [4], low-threshold nanolasers [5], quantum information processing [6], group delay [7], and photonic chips. The cavity *Q* factor per modal volume *V*, *Q*/*V*, determines the strength of various cavity interactions, and an ultra-small cavity enables large-scale integration along with single mode operation over a broad range of wavelengths. However, high-*Q* cavities with dimensions of the order of optical wavelengths are difficult to realize, since radiation losses are inversely proportional to cavity size. Therefore, high-*Q* photonic nanocavities are becoming a topic of growing interest [8-14].

Recently, we attempted to realize a high-*Q* cavity with modal volume *V* of the order of $(\lambda_0/n)^3$ using a point-defect cavity in a two-dimensional (2D) photonic crystal (PC) slab [see Fig. 1(b)], and produced a cavity having Q = 45,000 and $V = 7.0\times 10^{-14}\,\mathrm{cm}^3 = 0.69(\lambda_0/n)^3$ (where λ_0 is the wavelength of light in air) [13].

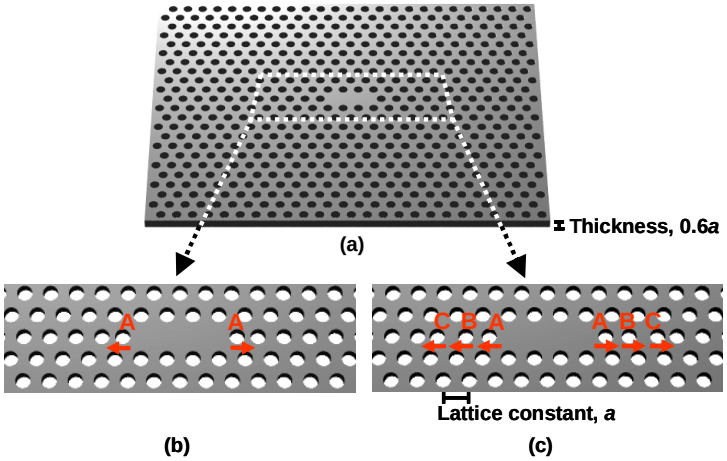

Fig. 1. (a) Schematic of the point-defect nanocavity in a 2D photonic crystal (PC) slab. The base cavity structure is composed of three missing air holes in a line. The PC structure has a triangular lattice of air holes with lattice constant *a*. The thickness of the slab and the radius of the air holes are 0.6*a* and 0.29*a*, respectively. (b)The designed cavity structure created by displacing two air holes at both edges in order to obtain high-*Q* factor (see Ref. 13). (c) The designed cavity structure created by fine-tuning the positions of six air holes near both edges to obtain an even higher *Q* factor.

We also discovered an important design rule for obtaining high-*Q* nanocavities. The envelope function of the electric field profile in the cavity is important for achieving strong optical confinement in a small area. The envelope function of the in-plane mode profile in the cavity should vary gently but remain spatially localized (like a Gaussian function) in order to increase the *Q* factor, whilst retaining a small *V*. For a point-defect cavity in a 2D PC slab, the photonic-bandgap effect is used to confine light in the in-plane direction, and total internal reflection (TIR) at the slab-air clad interface confines light in the vertical direction. For this

#6356 - $15.00 US Received 19 January 2005; revised 9 February 2005; accepted 11 February 2005

structure, TIR in the vertical direction is crucial for the realization of high-*Q* nanocavities. However, when there is an abrupt change in the electric field distribution of the cavity, the TIR condition at the cavity-air clad interface can not be fulfilled. Application of the above-mentioned rule to the cavity design allows the TIR condition to be fulfilled sufficiently so that out-of-slab light leakage is suppressed even in the case of very small *V*. Therefore, we tailored the envelope function of the electric field profile in the point-defect cavity of the 2D-PC slab by displacing two air holes at both cavity edges as shown in Fig. 1(b), so that the results of Ref. 13 were obtained.

In this paper, we theoretically and experimentally investigate further increasing the cavity *Q* factor by tailoring the envelope function of the electric field profile through fine-tuning of the positioning of six air holes near the cavity edges, as shown in Fig. 1(c). The paper is separated into five sections: Section 2 describes the strategy for cavity design, the procedure for calculation of cavity *Q* factor and theoretical results. Section 3 outlines sample fabrication. In Section 4 the experimental procedure is described before the measured results are presented and discussed. Finally, Section 5 provides some conclusions.

2. Design of high-*Q* nanocavity

2.1 Strategy for cavity design

In order to explain reasons why we fine-tune the positions of six air holes near both edges of the cavity, as shown in Fig. 1(c), it is important to discuss in detail the reasons why the design rule described above is effective in realizing a high-*Q* nanocavity. As previously mentioned, it is crucial to fulfill TIR conditions at the slab-air clad interface in order to increase the *Q* factor of the point-defect cavity in the 2D PC slab. Light confined in a very small cavity consists of numerous plane wave components with a range of wavevector (**k**) magnitudes and directions. The tangential component of the **k**-vector ($|k_{//}|$) at the slab-air clad interface determines whether or not the TIR condition for these wave components is fulfilled. When $|k_{//}|$ of each plane wave lies within the range 0- $2\pi / \lambda_0$, the wave can escape from the cavity to the air clad because the conservation law for $|k_{//}|$ is fulfilled at the interface. On the other hand, when $|k_{//}|$ in the cavity is larger than $2\pi / \lambda_0$, light is strongly confined inside the cavity because the conservation law for $|k_{//}|$ at the interface is not fulfilled (or the TIR condition is fulfilled). $|k_{//}|$ for each plane wave can be obtained by spatial Fourier transformation (FT) of the in-plane electric field at the surface of the slab. Therefore, we calculated the in-plane electric field distribution E_y at the surface of the slab. The electric field distribution E_y, calculated using the three-dimensional (3D) finite-difference time-domain (FDTD) method, for the fundamental resonant mode of the cavity without a displacement of the air holes at the surface of the slab is shown in Fig. 2(a). It is clear that the electric field is concentrated in the center of the cavity so that it resembles a one-dimensional (1D) cavity resonating along the center line. Therefore, to simplify the evaluation of the cavity mode, we focused on the electric field (E_y) along the center line at the slab surface. This E_y profile is given by the solid line in Fig. 2(b) and the FT of the electric field profile is shown by the solid line in Fig. 2(c). The gray area around $|k_{//}| = 0$ in Fig. 2(c) represents the leaky region or light cone, where the conservation law for $|k_{//}|$ is fulfilled at the cavity-air clad interface, leading to out-of-slab leakage of light as described above. As shown in Fig. 2(b), most components are observed outside the leaky region whilst some components do exist inside, which decreases the *Q* factor of the cavity.

We now consider reasons why some components of the cavity mode exist inside the leaky region. An electric field profile in a cavity can be expressed as a product of a fundamental sinusoidal wave of wavelength λ and an envelope function determined by the cavity structure. The fundamental wave gives a delta function FT spectrum with two peaks at k $= \pm 2\pi / \lambda$, while the envelope modifies the spectrum.

#6356 - $15.00 US Received 19 January 2005; revised 9 February 2005; accepted 11 February 2005

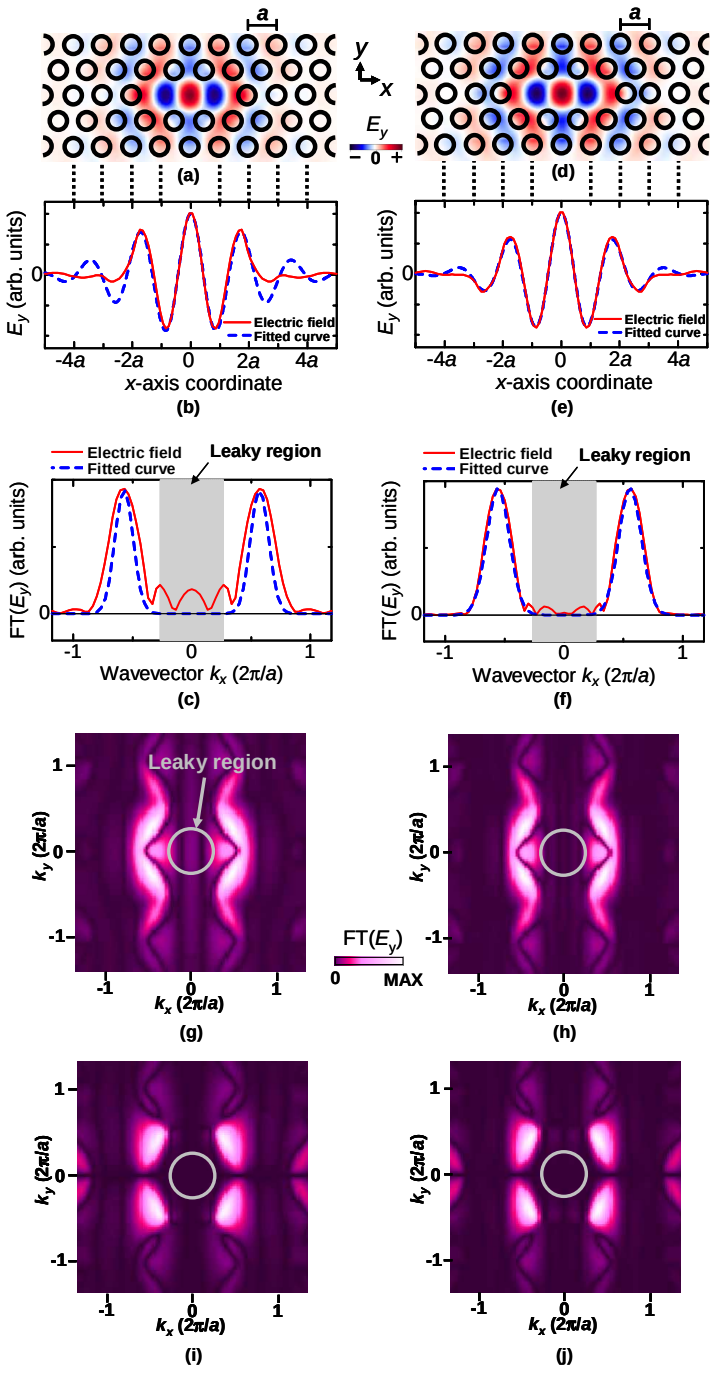

Fig. 2. (a) The electric field distribution (E_y) of the fundamental mode for a cavity without air hole displacement at both edges. (b) The profile of (a) along the center line of the cavity and the fitted curve corresponding to the product of a fundamental sinusoidal wave and a Gaussian envelope function. (c) The 1D FT spectra of (b). The leaky region or light cone is indicated by the gray area. (d), (e), (f) The electric field distribution (E_y), the E_y profile at the center line and the fitted curve, and the 1D FT spectra, respectively, for the cavity structure shown in Fig. 1(b). The displacement of air holes at the edges is set at 0.20a. (g), (h) The 2D FT spectra of (a) and (d), respectively. (i), (j) The 2D FT spectra of E_x for cavities of (a) and (d), respectively.

#6356 - $15.00 US Received 19 January 2005; revised 9 February 2005; accepted 11 February 2005

As shown in Fig. 2(c), the fundamental wave of this cavity has the peaks outside the leaky region, while the envelope function generates some plane wave components inside the leaky region. It is clear that the *Q* factor of this cavity is therefore strongly dependent upon the envelope function.

A fitted curve corresponding to the product of the same fundamental sine wave and a Gaussian envelope function is also shown, as a broken line in Fig. 2(b). As Fig. 2(c) shows, the FT spectrum of this curve has very few leaky components. The differences in the leaky components of the cavity mode and the fitted curve are due to the differences in the FT spectra of the two envelope functions. As can be seen in Fig. 2(b), it is found that the envelope of the cavity mode varies more abruptly than the Gaussian function at the cavity edge. This abrupt change generates other wavevector components in Fourier space which lie inside the leaky region.

Therefore, in order to obtain a high-*Q* cavity, it is important to avoid abrupt changes in the envelope function at the cavity edge. However, it is also clear that confinement to regions having dimension of the order of optical wavelengths requires a spatially localized envelope function of these dimensions. Therefore, in order to realize a high-*Q* photonic nanocavity, the envelope function should be gently varying but remain spatially localized. As shown here, a Gaussian function can fulfill both conditions. Some other functions, such as Lorentzians can also fulfill both conditions.

In Ref. 13, in order to minimize differences between the electric field profile in the cavity and the fitted curve using the Gaussian envelope function at the cavity edge as shown in Fig. 2(b), the air hole positions at the cavity edges were adjusted to lie slightly outside the cavity, as shown in Fig. 1(b). Reflections at the cavity edge are expected to be weakened by disturbing the periodicity of the air holes and therefore the Bragg reflection condition. The electric field distribution calculated for a cavity structure with an air hole displacement of 0.20*a*, where *a* is the lattice constant of the PC, is shown in Fig. 2(d). The electric field profile along the center line and the fitted curve are shown in Fig. 2(e). The FT spectra are shown in Fig. 2(f). As shown in Fig. 2(e), confinement is reduced and the electric field penetrates further outside the cavity, so that the electric field profile of the cavity is more similar to the fitted curve of the Gaussian envelope function, than that of the original cavity without air hole displacement. As can be clearly seen in Fig. 2(f), the leaky components for this cavity are dramatically reduced in comparison with those of the original cavity shown in Fig. 2(c). This means that air hole displacement can be expected to significantly increase the cavity *Q* factor. The *Q* factor of the structure was actually increased by a factor of 10 as shown in Ref. 13.

A closer examination of the two curves in Fig. 2(e) shows that, even in the case of the electric field profile of the cavity with an air hole displacement of 0.20*a*, some discrepancy between the mode profile and the fitted curve exists outside the cavity, including at the neighboring air holes (position A in Fig. 1(b)). A reduction in this discrepancy is expected to further increase the *Q* factor of the cavity. In this work, we theoretically and experimentally extend the investigation to cavities with air hole displacements also at positions B and C as shown in Fig. 1(c).

In addition, in this work, the 1D E_y profile and 1D-FT spectrum along the *x*-axis are used to evaluate cavity characteristics. The reason why it is not important to consider the profile along the *y*-axis is as follows: Fig. 2(g) and (h) show the 2D-FT spectra of the electric field distributions E_y of Fig. 2(a) and (d), respectively, where the leaky regions lie inside the gray circles. As can be seen in Fig. 2(g) and (h), the fundamental wave is outside the leaky region and just on the k_x axis. Broadening of the wavevector distribution along the k_x and k_y directions in Fourier space is determined by the electric field distributions along the *x*- and *y*-axis in real space, respectively. Therefore, it is clear that leaky components are generated by the distribution E_y along not the *y*-axis but the *x*-axis direction in real space. The electric field E_x is not considered because very few components inside the leaky region are seen in the FT spectra of E_x, as shown in Fig. 2(i) and (j), which represents E_x of the cavities without shift and with 0.20*a* shift of air holes.

#6356 - $15.00 US Received 19 January 2005; revised 9 February 2005; accepted 11 February 2005

2.2 Calculation procedure

We calculated the *Q* factors for cavities with a range of air hole displacements at positions A, B and C. The 3D-FDTD method was used to calculate the *Q* factors. The structure was discretized on a 3D mesh and Mur's second-order absorbing-interface condition was applied to the outer surface of the computational domain. The base 2D-PC slab is composed of Silicon with a triangular lattice of air holes having lattice constant *a*. The parameters used here included a slab thickness of 0.6*a*, air hole radius of 0.29*a*, slab index of 3.4 and an air clad index of 1. The point-defect cavity in the 2D-PC slab was made as shown in Fig. 1. The size of PC layer surrounding the cavity is ±25*a* in the *x*-direction and $\pm 7\sqrt{3}a$ (= ±14 rows) in the *y*-direction. (We have confirmed that the *Q* factor determined by the in-plane loss through the PC layer is much larger than 10^7).

Next, we describe the methods used to calculate the *Q* factors of the cavity modes. The *Q* factor is expressed as follows:

$$Q \equiv \omega_0 \frac{U(t)}{-dU(t)/dt}, \tag{1}$$

where ω_0 is the angular frequency of the cavity mode, and $U(t)$ is the total energy stored in the cavity. Equation (1) can be used to derive the following equation:

$$U(t) = U(0)\exp[-(\omega_0 t)/Q], \tag{2}$$

and, for example, the magnetic field $H(t)$ can be expressed as follows:

$$\ln[H(t)] = \ln[H(0)] - [\omega_0/(2Q)]t. \tag{3}$$

As can be seen in Eq. (3), the *Q* factor can be calculated by measuring the slope of the exponential decay of the magnetic field (or the electric field) of a given cavity mode. We calculated the *Q* factor from the slope and ω_0 derived using the FT of $H(t)$. This method is useful for relatively low *Q* factors. However, for higher *Q* factors, the slope $\omega_0/(2Q)$ is very small which will result in larger errors. By employing an alternative method, the calculated value was checked. The second method calculates both the energy losses radiated from an interface surrounding the cavity and the energy stored in the cavity. The *Q* factor is determined by substituting both values into Eq. (1). For the cavity modes of the structures analyzed in this section we found little discrepancy between the two methods, suggesting that the results calculated in this work are valid.

In addition, we estimated the modal volume of the cavities by inserting the calculated electric field distributions into the following equation [5,9]:

$$V = \frac{\int \varepsilon(\mathbf{r})|E(\mathbf{r})|^2 d^3\mathbf{r}}{\max[\varepsilon(\mathbf{r})|E(\mathbf{r})|^2]}, \tag{4}$$

where $\varepsilon(\mathbf{r})$ is the dielectric constant and $E(\mathbf{r})$ is the electric field. The integration region in Eq. (4) is ±14*a* in the *x*-direction, $6\sqrt{3}a$ (= ±12 rows) in the *y*-direction, and ±4.3*a* in the *z*-direction from the center of the cavity. We have confirmed that the size of the region is sufficiently large for calculating Eq. (4).

2.3 Calculated results for cavity Q factor and modal volume

The methods described above were used to calculate the *Q* factor and modal volume of cavities with a range of displacements of air holes at position A (the nearest neighbors). The results are shown in Fig. 3(a) as a function of air hole shift. As the air holes are displaced, the

#6356 - $15.00 US Received 19 January 2005; revised 9 February 2005; accepted 11 February 2005

Q factor increases drastically and then decreases as well, in agreement with our previous results [13].

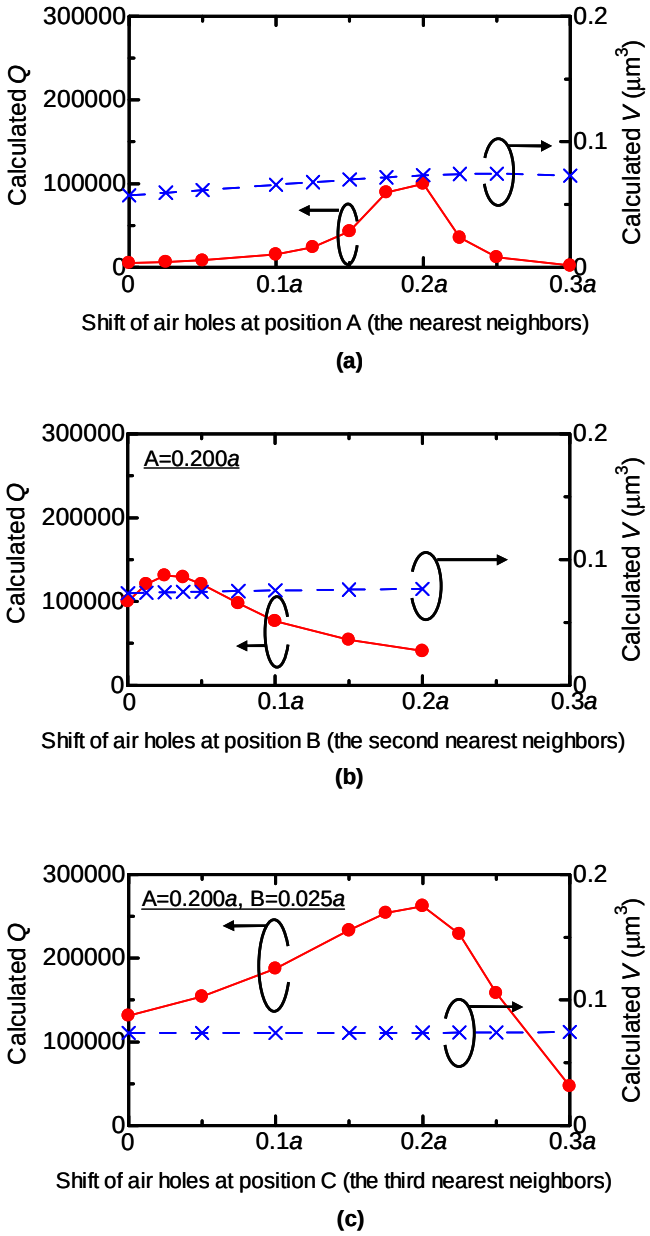

Fig. 3. (a) Cavity *Q* factors and the modal volume (*V*) obtained theoretically for cavities with a range of displacements of air holes at position A (the nearest neighbors). (b) Those for cavities with a range of displacements of air holes at position B (the second nearest neighbors), whilst fixing the position of air holes A at their optimum value of 0.200*a*. (c) Those for the cavities with a range of displacements of air holes at position C (the third nearest neighbors), whilst fixing the positions of air holes A and B at their optimum values of 0.200*a* and 0.025*a*, respectively.

#6356 - $15.00 US Received 19 January 2005; revised 9 February 2005; accepted 11 February 2005

The reason why *Q* factor increases with displacing air holes is because the envelope function of the electric field profile of the cavity approaches a Gaussian function as described in Sec. 2.1. On the other hand, when the holes are displaced too much, the electric field penetrates more outside the displaced holes. Then the optical confinement becomes more gradually around the holes, while the electric field distribution decays abruptly outside the holes. Therefore, the envelope function of the electric field profile of the cavity deviates from Gaussian function. Most likely due to this deviation *Q* factor of the cavity decreases with displacing air holes too much. The maximum *Q* factor, as large as 100,000, is obtained for an air hole displacement at position A of 0.200*a*. However, the calculated modal volume is found to be almost constant relative to the *Q* factors. One reason for this is likely to be that the displacement of the air holes is relatively small in comparison with the cavity size. It is also likely that since the electric field is concentrated around the center of the cavity as shown in Fig. 2(a) and (d), changes at the cavity edge have little effect on the modal volume.

Next, we displaced air holes at position B (the second nearest neighbors), while fixing the air holes at position A at the optimum displacement of 0.200*a*. The resulting *Q* factors and modal volumes calculated are shown in Fig. 3(b). As can be seen, the maximum *Q* factor, as large as 130,000, is obtained for a displacement of air holes B of 0.025*a*. This suggests that air hole displacements at position B can further increase the cavity *Q* factor. Moreover, we shifted the air-holes at position C (the third nearest neighbors), whilst fixing the positions of air-holes A and B at their optimum values. The results are shown in Fig. 3(c). The maximum *Q* factor, as large as 260,000, is obtained for a displacement of air holes C of 0.200*a*. This means that the displacement of air holes at position C results in a considerable increase in the cavity *Q* factor. The maximum *Q* factor calculated here is larger than that of the cavity without displaced air holes (5,200) by a factor of 50. However, Fig. 3(b) and (c) as well as Fig. 3(a) clearly show that calculated modal volumes are almost constant. The value *V* at the positions of air holes where maximum *Q* factor is obtained is as small as 7.4×10^{-14} cm^3 (= $0.73\,(\lambda_0 / n)^3$). This result clearly indicates that the *Q* factor of the photonic nanocavity can be increased significantly by tailoring the positions not only of air holes A but also of air holes B and C, whilst keeping the cavity volume small.

3. Fabrication

In order to practically test these theoretical results, we fabricated samples having various air hole displacements. Initially, a resist mask (ZEP-520) was coated onto a silicon-on-insulator (SOI) substrate. PC patterns were drawn on this resist mask by electron-beam lithography. The resist patterns were then transferred to the upper Silicon layer using inductively-coupled plasma reactive-ion etching (ICP/RIE). After the dry-etching procedure, the resist was removed using an O_2 plasma. Finally, the SiO_2 layer under the PC layer was selectively etched away using hydrofluoric (HF) acid to form an air-bridge structure. We selected a lattice constant *a* of 420 nm and for comparison used the same parameters as for the calculated structure for this fabricated structure. The PC area was $15\mu m\times 250\mu m$.

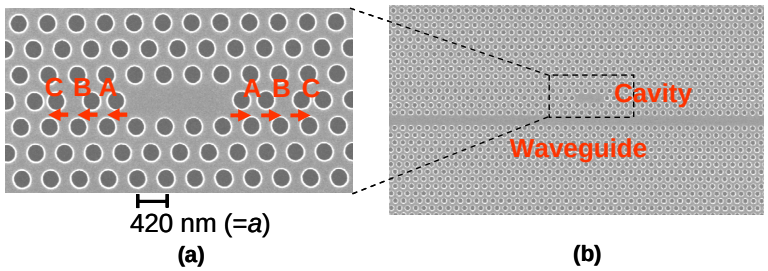

Fig. 4. SEM images of one of the fabricated samples, including the point-defect cavity with displaced air holes A, B, and C. (a) Magnified view of the point-defect cavity. (b) Top view of the sample. A line-defect waveguide was introduced near the point-defect cavity.

#6356 - $15.00 US Received 19 January 2005; revised 9 February 2005; accepted 11 February 2005

Scanning electron microscope (SEM) images of one of the fabricated samples, including the point-defect cavity with displacement of air holes A, B and C, are shown in Fig. 4(a) and (b). A line-defect waveguide was also introduced near the point-defect cavity, as shown in Fig. 4(b).

4. Experiment and discussion

4.1 Measurement procedure

Photons were injected from a line-defect waveguide facet and the cavities were excited via the waveguide. Light emitted from the cavity into free space and transmitted through the waveguide was observed, as shown in Fig. 5(a) and (b) which show transmission and radiation spectra, respectively. The insets in the figures show the geometry of these photon fluxes measured from the sample. From both spectra, it is possible to evaluate the cavity Q factor experimentally. It is important to note that the total Q factor (Q_{total}) obtained from the linewidth of the radiation spectrum shown in Fig. 5(b) is not the intrinsic Q factor of the cavity itself. The intrinsic Q factor, denoted Q_{v}, is determined by the coupling loss to free space only. On the other hand, Q_{total} is also affected by the coupling loss to the waveguide mode. Therefore, Q_{v} should be larger than the Q_{total}. As can be seen in Fig. 5(a), the transmittance drops dramatically at the resonant wavelength of the cavity, owing to the reflection and the loss originating from coupling to the point-defect cavity mode [2,15]. From coupled mode theory [2,15,16], Q_{v} can be expressed as follows:

$$Q_{\text{v}} = Q_{\text{total}} / \sqrt{T} \ , \tag{5}$$

where T is the transmittance at the resonant wavelength of the cavity. The transmittance T is defined as the ratio of the transmitting energy in the presence of the cavity near the waveguide to the energy in the absence of the cavity. Experimentally, we can evaluate T as T_2/T_1 (as shown in Fig. 5) [2]. We describe the detailed derivation of Eq. (5) in Appendix. Using the above relation, it is possible to experimentally evaluate the intrinsic Q factor of the cavity (Q_{v}).

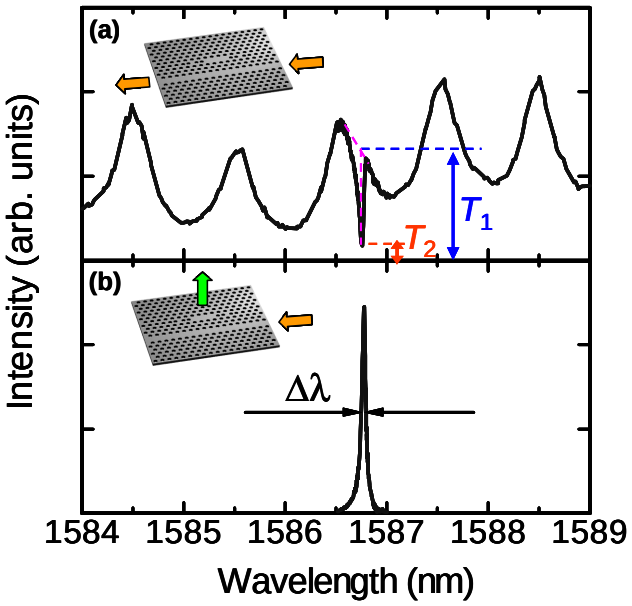

Fig. 5. An example of the measured spectra. (a), (b) Show transmission and radiation spectra, respectively. The insets in the figures show the geometry of the photon fluxes measured.

#6356 - $15.00 US Received 19 January 2005; revised 9 February 2005; accepted 11 February 2005

4.2 Measured results and discussion

At first, we displaced air holes at position A using finer steps than those used in Ref. 13, and measured Q_v using the above method. The results are shown in Fig. 6(a).

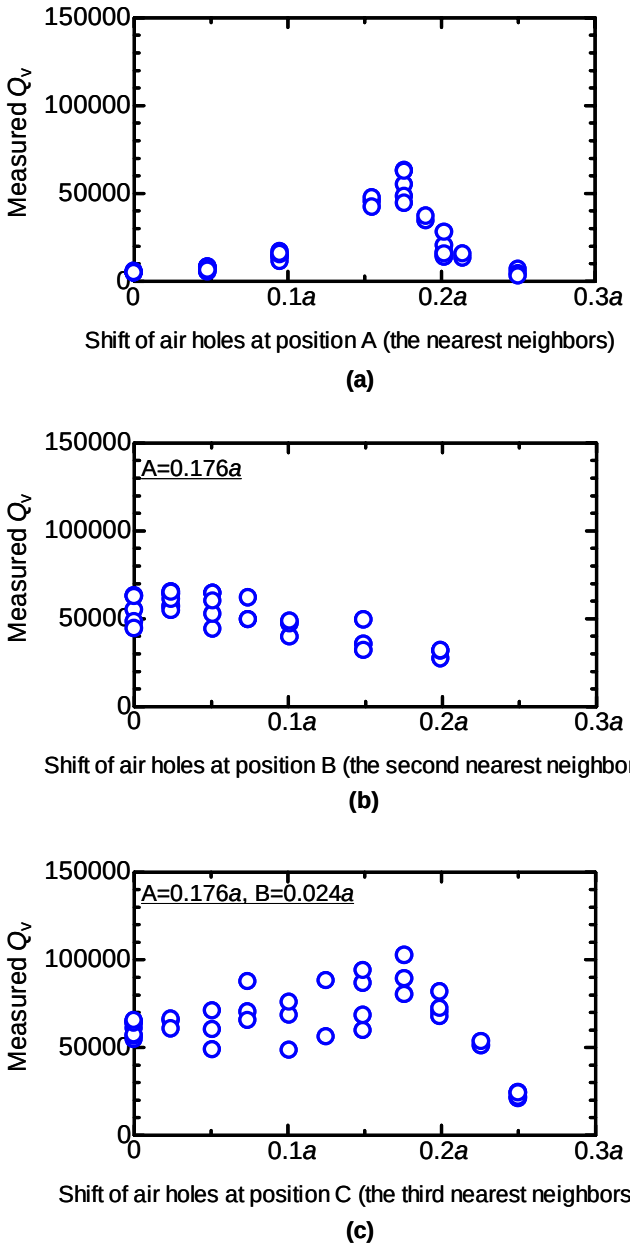

Fig. 6. (a) Cavity Q factors (Q_v) obtained experimentally for cavities with various displacements of air holes at position A. (b) Those for cavities with various displacements of air holes at position B, whilst fixing the position of air holes A at their optimum value of around 0.176a. (c) Those for the cavities with various displacements of air holes at position C, whilst fixing the positions of air holes A and B at their optimum values of around 0.176a and 0.024a, respectively.

#6356 - $15.00 US Received 19 January 2005; revised 9 February 2005; accepted 11 February 2005

As can be seen, for a fixed air hole displacement we measured various samples having different distances between the point-defect cavity and the line-defect waveguide, clearly demonstrating that reproducibility was very good. As the air holes are shifted, the *Q* factor increases drastically and then decreases as well, in agreement with earlier work [13]. A maximum Q_v of up to 63,000 is obtained for a displacement of air holes A of around 0.176*a*. Comparison with the calculated results (Fig. 3(a)) indicates that the theoretical and experimental results are qualitatively similar in terms of variations in Q_v as a function of air hole displacement. The experimental values are lower than theoretical ones, most likely due to fluctuations in the fabricated structures, including small perturbations and slightly angled etched sidewalls which could lead to scattering losses and coupling losses to TM-like slab modes [17], respectively.

Next, we displaced the air holes at position B whilst fixing the positions of air holes A at the optimum value of 0.176*a*. The measured Q_v values are shown in Fig. 6(b). You can see that the maximum Q_v is obtained by slightly shifting air holes B, resulting in a value as large as 65,000. Finally, we displaced air holes at position C whilst fixing positions of air holes A and B at their optimum values, and measured the *Q* factor of the cavities. The results shown in Fig. 6(c) show that a maximum Q_v value of up to 100,000 is obtained for an air hole C displacement of around 0.176*a*. This *Q* factor is larger than that of the initial cavity having no air hole displacement (5,000) by a factor of 20. These experimental results indicate that displacing the air holes at positions A, B, and C is a very effective method for significantly increasing cavity *Q* factors. The experimental results in Fig. 6 and the theoretical results in Fig. 3 are qualitatively very similar in terms of the variation of Q_v as a function of displacements of not only air holes A, but also for the displacements of air holes B and C.

The resonant (radiation) spectrum obtained for the optimum cavity with the maximum Q_v (100,000) is shown in Fig. 7. The linewidth is as narrow as 18 pm, which means that very high Q_{total} (88,000) is obtained. Therefore, we have successfully increased the cavity *Q* factor further by displacements of not only air holes at positions A, but also at positions B and C, as predicted.

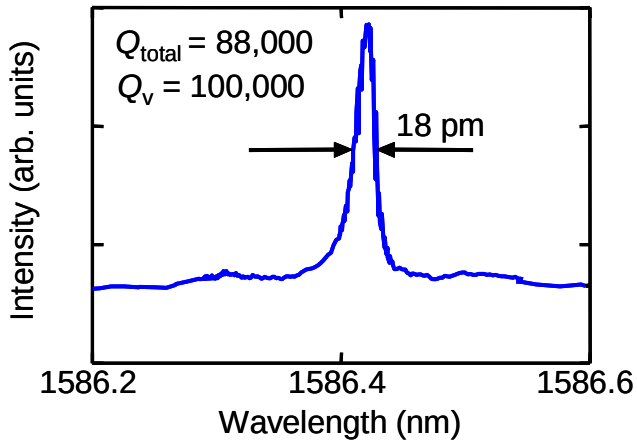

Fig. 7. The resonant (radiation) spectrum obtained for the optimum cavity with the maximum Q_v (100,000). The linewidth is as narrow as 18 pm, which means that very high Q_{total} (88,000) is obtained.

We now consider the *Q* factor per unit volume or *Q*/*V*, which is one of the figures of merit for photonic nanocavities. As mentioned in Section 2, the cavity modal volume *V* is almost constant when displacing air holes. The volume calculated for the cavity structure with the maximum Q_v is as small as 7.2×10^{-14} cm^3 ($= 0.71\,(\lambda_0 / n)^3$). Therefore, *Q*/*V* is as large as

#6356 - $15.00 US Received 19 January 2005; revised 9 February 2005; accepted 11 February 2005

1.4×10^{18} cm^{-3} = $1.4\times10^{5}(\lambda_0/n)^{-3}$, which is larger than that for the cavity without air hole displacement by a factor of 16 and larger than the maximum value for the cavity in previous work by more than a factor of two [13].

Finally, we compare the value of Q/V for this nanocavity with those of other reported nanocavities. Of all the experimental Q factors reported for PC nanocavities not fabricated by us, the highest Q_v is 40,000, where V is $0.9(\lambda_0/n)^3$ [14]. Q/V for this cavity is estimated to be $4.4\times10^{4}(\lambda_0/n)^{-3}$ which is smaller than that measured for the cavity fabricated in this work with maximum Q_v by a factor of three. In comparison with experimental Q factors reported for nanocavities not in PCs, the highest Q_v reported is 12,000 for a microdisk [18], where V is $4.8(\lambda_0/n)^3$ and so Q/V is $2.5\times10^{3}(\lambda_0/n)^{-3}$. This Q/V value is much smaller than for the above PC nanocavities. The maximum Q/V values reported for micropost [19] and microgear [20] cavities are $400(\lambda_0/n)^3$ and $600(\lambda_0/n)^3$, respectively, and much smaller than the above-mentioned microdisk. This clearly indicates that optical confinement by the photonic nanocavity fabricated in this work is much stronger than for any other nanocavity reported so far. For further drastic increases of Q/V, a new approach should be taken to obtain the perfect Gaussian curve for optical confinement, which will be reported elsewhere [21].

5. Conclusion

In summary, we fine-tuned the positions of air holes near the edge of the point-defect cavity in a 2D-PC slab according to a design rule which we discovered recently, that the envelope function of the mode profile in the cavity should gently vary but remain spatially localized. We have theoretically calculated that cavity Q factors can be increased significantly, and have succeeded in experimentally realizing a high-Q photonic nanocavity having Q_v of 100,000 and V of $0.71(\lambda_0/n)^3$. The Q/V of the obtained nanocavity is as large as $1.4\times10^{5}(\lambda_0/n)^{-3}$. This is larger than that of the cavity without any air hole displacement by a factor of 16 and is larger than those of any other reported nanocavities by a factor of three. The high-Q photonic nanocavity obtained in this work and the design rule theoretically and experimentally validated here could be utilized in many fields of science and engineering.

Acknowledgments

This work was partly supported by Core Research for Evolution Science and Technology (CREST), Japan Science and Technology Agency; and also by a Grant-in-Aid for Scientific Research and Information Technology program of the Ministry of Education, Culture, Sports, Science and Technology of Japan.

Appendix

We derive Eq. (5) from coupled mode theory. The schematic of the sample structure used for the evaluation of Q factor in this study is shown in Fig. 8.

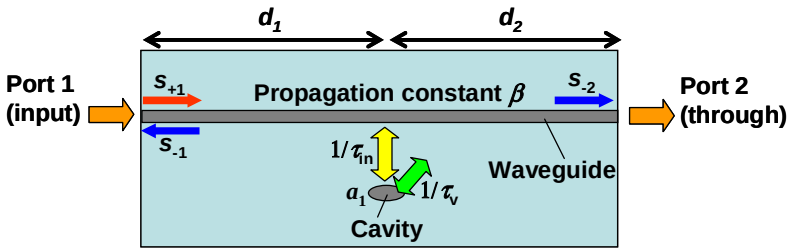

Fig. 8. Schematic of 2D PC slab including a cavity and a waveguide.

#6356 - $15.00 US Received 19 January 2005; revised 9 February 2005; accepted 11 February 2005

The amplitudes of the incoming wave coupled to the waveguide from port1 (input facet) and the outgoing wave reflected by the point-defect cavity to port 1 are denoted by S_{+1} and S_{-1}, respectively. The amplitudes of the outgoing wave to port 2 (output facet) and the cavity mode are denoted by S_{-2} and a_1, respectively. The decay rates from the cavity into the waveguide and into free space are denoted by $1/\tau_{in}$ and $1/\tau_v$, respectively. The decay rates are related to the in-plane Q (Q_{in}) and the vertical Q (Q_v) by $Q_{in} = \tau_{in}\omega_0/2$ and $Q_v = \tau_v\omega_0/2$. Then, the equations for the evolution of the cavity modes in time and the outgoing waves are given as follows [16]:

$$\frac{da_1}{dt} = (j\omega_0 - \frac{1}{\tau_v} - \frac{1}{\tau_{in}})a_1 + \sqrt{\frac{1}{\tau_{in}}}e^{-i\beta d_1}S_{+1} \tag{6}$$

$$S_{-1} = -\sqrt{\frac{1}{\tau_{in}}}e^{-i\beta d_1}a_1 \tag{7}$$

$$S_{-2} = e^{-i\beta(d_1+d_2)}\left(S_{+1} - \sqrt{\frac{1}{\tau_{in}}}e^{i\beta d_1}a_1\right) \tag{8}$$

Based on these equations, transmittance T from port 2 can be expressed by

$$T = \left|\frac{S_{-2}}{S_{+1}}\right|^2 = \frac{(\omega-\omega_0)^2 + \left(\frac{\omega_0}{2Q_v}\right)^2}{(\omega-\omega_0)^2 + \left(\frac{\omega_0}{2Q_v} + \frac{\omega_0}{2Q_{in}}\right)^2} \tag{9}$$

Under the condition of $\omega = \omega_0$, Eq. (9) becomes

$$T = \frac{\left(\frac{1}{Q_v}\right)^2}{\left(\frac{1}{Q_v} + \frac{1}{Q_{in}}\right)^2} \tag{10}$$

On the other hand, since the total loss from the cavity is equal to the sum of the radiation loss to free space and the coupling loss to the waveguide, total Q can be expressed as follows:

$$\frac{1}{Q} = \frac{1}{Q_v} + \frac{1}{Q_{in}} \tag{11}$$

Substituting Q_{in} from Eq. (11) into Eq. (10), we get the following Eq. (12).

$$T = \left(\frac{Q}{Q_v}\right)^2 \tag{12}$$

This Eq. (12) is equivalent to Eq. (5).

#6356 - $15.00 US Received 19 January 2005; revised 9 February 2005; accepted 11 February 2005